Proton-induced fission on ^{241}Am, ^{238}U, and ^{237}Np at intermediate energies

A. Deppman,* E. Andrade-II,† V. Guimarães,‡ and G. S. Karapetyan§
Instituto de Fisica, Universidade de São Paulo, P. O. Box 66318, 05389-970 São Paulo, SP, Brazil

A. R. Balabekyan‖
Yerevan State University, Alex Manoogian 1, Yerevan 0025, Armenia

N. A. Demekhina¶
Yerevan Physics Institute, Alikhanyan Brothers 2, Yerevan 0036, Armenia and Joint Institute for Nuclear Research (JINR), Flerov Laboratory of Nuclear Reactions (LNR), Joliot-Curie 6, Dubna 141980, Moscow, Russia
(Received 11 April 2013; published 14 August 2013)

Intermediate energy data of proton-induced fission on ^{241}Am, ^{238}U, and ^{237}Np targets were analysed and investigated using the computational simulation code CRISP. Inelastic interactions of protons on heavy nuclei and both symmetric and asymmetric fission are regarded. The fission probabilities are obtained from the CRISP code calculations by means of the Bohr-Wheeler model. The fission cross sections, the fissility and the number of nucleons evaporated by the nuclei, before and after fission, are calculated and compared with experimental data. Some of the model predictions agree completely with the data. We conclude that our two step model of the CRISP code provides a good description of intermediate energy proton-induced fission.

DOI: 10.1103/PhysRevC.88.024608 PACS number(s): 25.85.Ge

I. INTRODUCTION

The interaction between high energy protons and atomic nuclei has been a subject of study over the last 70 years. Such a continuous interest in this subject is caused by many reasons. First of all, proton-induced nuclear reactions involve fundamental problems; the nucleon-nucleon interaction and the properties of the nuclei in various conditions of excitation. Modification of the proton energy and/or target nucleus leads to a rich spectrum of phenomena, which have to be understood and described theoretically. In addition, since high energy proton collisions with atomic nuclei do not cause significant compression of the nuclei, the description of proton-induced reactions is less complex than those induced by heavier ions, and therefore can be useful in the comprehension of reactions induced by the latter probes.

The study of the proton-nucleus collision is a source of information for scientific and technological applications, as for instance, medical physics applications and nuclear reactor technologies. However, a broad range of proton energies, from a few MeV to tens of GeV and a full list of target nuclei must be studied. At the present, the situation, experimentally as well as theoretically, is rather puzzling. Despite a long history of investigations of proton-nucleus reactions, neither the predictive power of the available theoretical models provides the demanded accuracy, nor the experimental databases are rich enough to serve as benchmarks, which may put very restrictive demands and constraints on the theoretical description.

In the case of the fission process, a comparison of calculations with the measured charge, mass, energy, and spin distributions of the fragments, as well as the systematization of the experimental data within various model representations, can provide relevant information about the properties of primary fragments and the mechanism of their formation. The present work aims to show the results of the calculations using the CRISP code with multimodal model in describing proton-induced fission at 660 MeV on heavy targets (^{241}Am, ^{238}U, ^{237}Np). The data considered here are from the experiments of Refs. [1] and [2].

II. METHODOLOGY

Presently, the only way a complete description of particle collisions, in a large range of incident energy and on target nuclei with the mass varying from light nuclei as carbon to heavy nuclei as Americium, can be achieved, is by considering simulation with a Monte Carlo method. In this work we use the Monte Carlo simulation code CRISP to calculate the nuclear processes triggered by the inelastic interaction of protons with heavy target nuclei. This code has been developed for more than ten years [3–9] and it has been applied in the study of fission induced by photons, electrons and protons, and for the study of hyper-nucleus decay [10]. Also, it has been used in the development of new nuclear reactor technologies [11–13].

The main feature of this Monte Carlo code is the precise description of the intranuclear cascade, where a time-ordered sequence of collisions is governed by strict verification of the Pauli principle in a square-well nuclear model. In this case, pre-equilibrium emissions are naturally considered until the complete thermalization of the nucleus. After the intranuclear cascade is finished, the competition between evaporation and fission is described by using the Weisskopf-Ewing model [14], until the nucleus is too cold to emit any other particle. The

*deppman@if.usp.br
†esegundo@if.usp.br
‡valdirg@if.usp.br
§ayvgay@ysu.am
‖balabekyan@ysu.am
¶demekhina@nrmail.jinr.ru

electroweak decay will then lead the nuclear system to its final ground state, although this step of the reaction is not considered in this work.

In each step of the evaporation chain, the nuclear excitation energy is recalculated by

$$E_x^{(f)} = E_x^{(i)} - (B + V + \varepsilon), \tag{1}$$

where $E_x^{(f)}$ and $E_x^{(i)}$ are the excitation energy of the final and initial nucleus, respectively, B is the evaporated particle separation energy, V is its Coulomb potential, and ε is the mean kinetic energy of the emitted particle, which is fixed at 2 MeV. Also, the fission channel is considered at each step with branching ratios given by the Bohr-Wheeler model. In the case of fission, the fragments are generated by following the multimodal random neck rupture model (MM-NRM) [15].

Theoretically, the fission process has been successfully described by the MM-NRM [15], which takes into account the collective effects of nuclear deformation during fission with the liquid-drop model, and includes single-particle effects through microscopic shell-model corrections. The microscopic corrections create valleys in the space of elongation and mass number, each valley corresponding to one different fission mode. The yield of a fragment, characterized by the fragment mass number A and the atomic number Z, is determined for each mode by a Gaussian distribution.

In the following we consider that fission can take place through three modes: a symmetric mode (superlong) and two asymmetric modes (standards I and II). The description of fission fragment formation allows us to understand the influence of the nuclear structures on the nature of fission. For instance, superlong mode fragments are strongly elongated with masses around $A_f/2$, where A_f is the mass of the fissioning nucleus with $A_f = A_H + A_L$, where the index H and L stand for the heavy and light fragment in a fission, respectively. Standard I mode is characterized by the influence of the spherical neutron shell $N_H \sim 82$ and proton shell $Z_H \sim 50$ in the heavy fragments with masses $M_H \sim 132$–134. The investigation of the influence of shell effects and pairing correlations on the fission-fragment mass and nuclear-charge distributions was performed by Schmidt *et al.* [16], where an indication of the proton shell closure $Z = 54$ effect was observed. Standard II mode is characterized by the influence of the deformed neutron shell closure $N_H = 86$–88 and proton shell $Z_H \sim 52$ in the heavy fragments with masses $M_H \sim 138$–140, A similar approach was recently used to study photon-induced fission [17–20].

In the multimodal model, the fission cross section, as a function of mass number, is obtained by the sum of the three Gaussian functions corresponding to the three modes mentioned above [21]:

$$\sigma_A = \frac{1}{\sqrt{2\pi}}\left[\frac{K_{1AS}}{\sigma_{1AS}}\exp\left(-\frac{(A - A_S - D_{1AS})^2}{2\sigma_{1AS}^2}\right) + \frac{K'_{1AS}}{\sigma'_{1AS}}\exp\left(-\frac{(A - A_S + D_{1AS})^2}{2\sigma_{1AS}'^2}\right) + \frac{K_{2AS}}{\sigma_{2AS}}\exp\left(-\frac{(A - A_S - D_{2AS})^2}{2\sigma_{2AS}^2}\right) + \frac{K'_{2AS}}{\sigma'_{2AS}}\exp\left(-\frac{(A - A_S + D_{2AS})^2}{2\sigma_{2AS}'^2}\right) + \frac{K_S}{\sigma_S}\exp\left(-\frac{(A - A_S)^2}{2\sigma_S^2}\right)\right], \tag{2}$$

where A_S is the mean mass number determining the center of Gaussian functions; and K_i, σ_i, and D_i are the contribution, dispersion and position parameters of the ith Gaussian functions. The indexes AS, S designate the asymmetric and symmetric components.

The CRISP code works on an event-by-event basis, and therefore the parameter A_S in Eq. (1) is completely determined by the mass of the fissioning nucleus A_f, that is, $A_S = A_f/2$. The quantities $A_S + D_{iAS} = A_H$ and $A_S - D_{iAS} = A_L$, where A_H and A_L are the masses of the heavy and light fragment, respectively, determine the positions of the heavy and light peaks of the asymmetric components on the mass scale. The value of $A_S = (A_H + A_L)/2$ is treated as the mass of the nuclei that undergo fission in the respective channel.

One important observable of the fission process is the charge distribution of a given isobaric chain with mass number A. It is assumed that this fission fragment charge distribution is well described by a Gaussian function characterized by the most probable charge, Z_p of an isobaric chain A (centroid of the Gaussian function) and the associated width parameter, Γ_z of the distribution as follows [22,23]:

$$\sigma_{A,Z} = \frac{\sigma_A}{\Gamma_z \pi^{1/2}}\exp\left(-\frac{(Z - Z_p)^2}{\Gamma_z^2}\right), \tag{3}$$

where $\sigma_{A,Z}$ is the independent cross section of the nuclide Z, A. The values σ_A correspond to the total fission cross section of a given isobaric chain with mass number A. The values Z_p and Γ_z can be represented as slowly varying linear functions of the mass number of the fission fragments:

$$Z_p = \mu_1 + \mu_2 A\,, \tag{4}$$

and

$$\Gamma_z = \gamma_1 + \gamma_2 A\,. \tag{5}$$

The values for these parameters obtained by a fitting procedure from Refs. [1,2] are $\mu_1 = 4.1$, $\mu_2 = 0.38$, $\gamma_1 = 0.92$, and $\gamma_2 = 0.003$ for ^{241}Am and $\mu_1 = 5.0$, $\mu_2 = 0.37$, $\gamma_1 = 0.59$, and $\gamma_2 = 0.005$ for ^{237}Np. In the present work, we applied the same values obtained for ^{241}Am to ^{238}U.

Analysis using Eqs. (2), (3), (4), and (5) has been performed with success to describe fission induced by different probes; thermal neutrons [24,25], protons up to energies of 190 MeV [23,26], 200 MeV neutrons [27], and heavy ions [28,29]. In these works, the yield, position, and width parameters for each mode in Eq. (2) were considered as free parameters in the fitting procedure. Here we use the multimodal model associated with the Monte Carlo code CRISP, which simulates

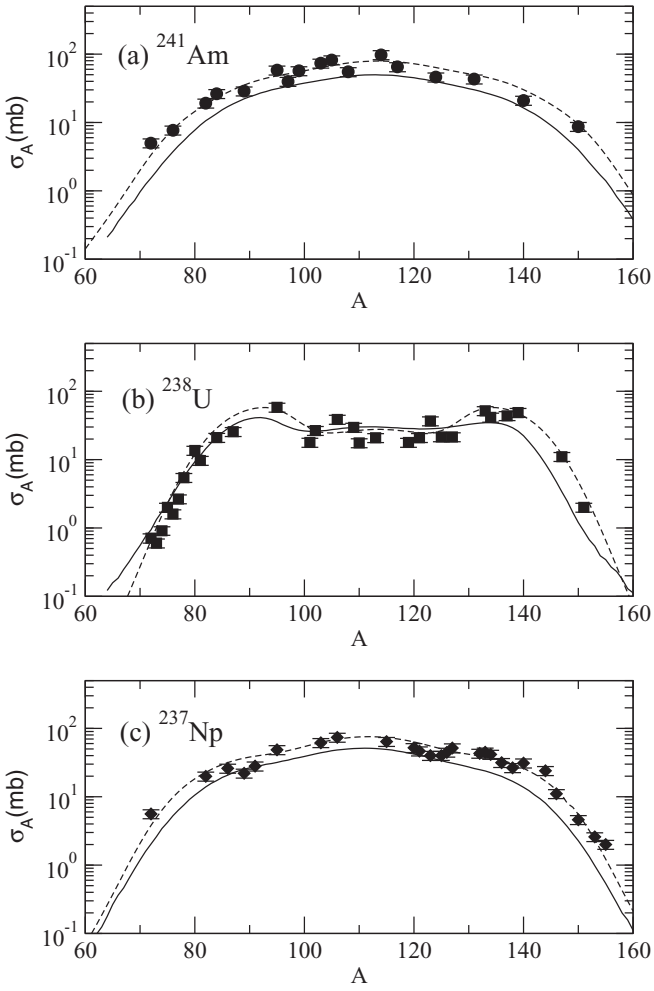

FIG. 1. Mass distributions of fission fragments induced by protons at $E_p = 660$ MeV on (a) ^{241}Am, (b) ^{238}U, and (c) ^{237}Np targets. The solid symbols; square, circle, and triangle are the experimental cross sections in units of mb for each of the indicated targets as a function of the isobaric chain A. The solid black line corresponds to the calculation by the CRISP code and the dotted line gives the results of a minimum χ-square fitting over the experimental data from Refs. [1] and [2].

the entire process up to the point of fission. In the CRISP code, the fissioning nucleus of all events is known and, therefore, the mass of the perfectly symmetric fission fragments is given by $A_S = A_f/2$.

Whenever the fission channel is chosen, the masses and atomic numbers of the heavy fragments produced, A_H and Z_H, respectively, are sorted according to Eq. (3). The light fragments are obtained according to $A_L = A_f - A_H$ and $Z_L = Z_f - Z_H$, where Z_f is the atomic number of the fissioning system.

As a final step, all fragments obtained go into a final evaporation step according to the model of evaporation/fission competition already mentioned. The energy of each fragment is determined using

$$E_i = \frac{A_i}{A_f} E_{\text{frag}}, \tag{6}$$

TABLE I. Parameters for the mass distribution calculations.

Parameter	^{241}Am	^{238}U	^{237}Np
K_{1AS}	45.0	53.80	49.0
K'_{1AS}	45.8	52.00	49.0
σ_{1AS}	4.2	1.60	4.5
σ'_{1AS}	4.2	1.71	4.5
D_{1AS}	20.0	22.50	21.3
K_{2AS}	220.5	477.32	252.0
K'_{2AS}	220.5	476.52	252.0
σ_{2AS}	7.0	4.29	6.5
σ'_{2AS}	7.0	4.19	6.5
D_{2AS}	25.5	22.90	26.3
K_S	2970.0	1396.45	2590.0
σ_S	15.0	14.2	13.7

where E_i and A_i are the excitation energy and the mass number of the fragment i, respectively. E_{frag} is the total excitation energy of the fragments, which is assumed to be equal to the excitation energy of the fissioning system.

Recently, this method of simulating fission reactions was used in the analysis of photofission with bremsstrahlung photons at end-point energies 50 MeV and 3500 MeV on ^{238}U and ^{232}Th targets, with satisfactory results [30].

III. RESULTS AND DISCUSSION

A. Mass distribution

The results for fragment mass distributions obtained with the CRISP code are presented in Fig. 1. Results of the best fitted distributions from Refs. [1,2] are also shown in the figure for comparison. The calculated results from the CRISP code are obtained with the parameters shown in Table I. As can be observed, both fit and calculated distributions reproduce the shape of the experimental distributions. The calculated position and width of the peaks for symmetric and asymmetric modes are in fair agreement with the experimental distributions. However, the calculated distributions by the CRISP code are systematically below the data for the ^{241}Am and ^{237}Np targets, indicating that the calculations for total fission cross sections underestimate the experimental cross sections.

The experimental total fission cross section is estimated by

$$\sigma_F^{\text{exp}} = \frac{1}{2} \sum_i \sigma^{\text{exp}}(A_i), \tag{7}$$

where $\sigma^{\text{exp}}(A_i)$ is the experimental cross section for each mass number A, where the factor $\frac{1}{2}$ has to be considered to avoid double counting of fission events due to the summation over the fragments.

The CRISP code calculates the total fission cross section by supposing that it is given by $\sigma_F^{\text{calc}} = D\sigma_{\text{in}}$, where D is the nuclear fissility and σ_{in} is the total cross section for the inelastic interaction. The CRISP code adopts the geometrical cross section to estimate the inelastic cross sections:

$$\sigma_{\text{in}} \sim \sigma_g = \pi(r_0 + r_0 A^{1/3})^2 . \tag{8}$$

TABLE II. Calculated and experimental quantities.

Parameter	^{241}Am	^{238}U	^{237}Np
$(\sigma_{tot})_{exp}$(barn)	1.76 ± 0.30	1.23 ± 0.18	1.60 ± 0.24
$(\sigma_{tot})_{cal}$(barn)	1.08	0.95	1.07
$(A_S)_{exp}$	113.5 ± 0.6	113.5 ± 0.6	111.7 ± 0.9
$(A_S)_{cal}$	113.0	114.0	111.5
$(A_f)_{exp}$	227.0	227.0	223.4
$(A_{ff})_{cal}$	226.0	228.0	223.0
$(A_f)_{cal}$	237.7	232.5	234.7
$(A_{comp})_{cal}$	238.9	233.0	234.9
(pre-scission neutrons)$_{cal}$	4.3	6.5	3.3
(post-scission neutrons)$_{cal}$	11.7	4.5	11.7
(evaporated neutrons)$_{exp}$	15 ± 2	12 ± 2	15 ± 2

In the geometric cross section, the nucleus is considered as a sphere with radius $R(A) = r_0 A^{1/3}$ and the proton as a sphere with radius r_0, where $r_0 = 1.2$ fm. The values for both experimental and calculated total fission cross sections obtained are shown in Table II. The ratios between calculated and experimental total fission cross sections $\sigma_F^{calc}/\sigma_F^{exp}$ are 0.6 ± 0.1, 0.8 ± 0.1, and 0.7 ± 0.1, respectively for ^{241}Am, ^{238}U, and ^{237}Np.

The calculated and experimental fissility, determined as the ratio $D = \sigma_F/\sigma_{in}$, for proton-induced fission on ^{241}Am, ^{238}U, and ^{237}Np targets as a function of the parameter Z^2/A are plotted in Fig. 2 together with estimated experimental values for protons [1,2] and photons [31,32] on ^{238}U and ^{232}Th targets. As can be noticed, the fissilities for fission induced by protons and photons on different targets and at different incident energies are below unity, and show a plateau of saturation for incident energies above ~40 MeV [33–35]. We can also observe in this figure that calculated fissilities with the CRISP code are close to unity and above the experimental values. A possible explanation for this behavior is the fact that the total

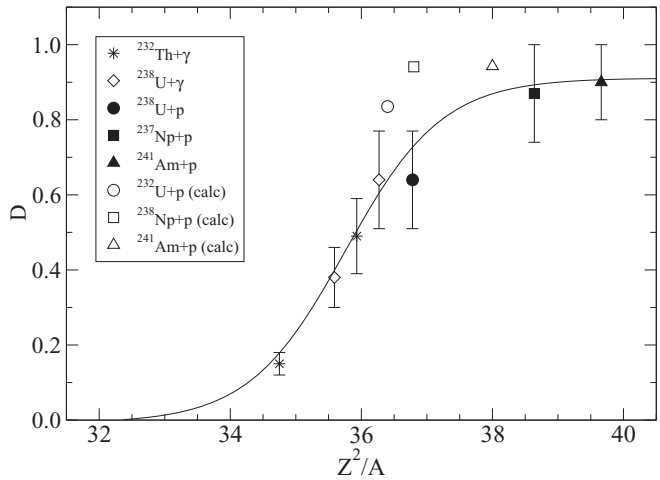

FIG. 2. Fissility D as a function of Z^2/A for $p + ^{237}$Np, $p + ^{238}$U, and $p + ^{241}$Am (calculated from the present work and experimental data from Refs. [1,2]), $\gamma + ^{238}$U and $\gamma + ^{232}$Th from Refs. [31,32], as indicated. Calculations by CRISP are open symbols without error bars. The solid line is to guide the eye to the experimental points.

inelastic proton-nucleus cross section is being underestimated. The quantitative difference can be attributed to the geometrical approximation given by Eq. (8), which assumes that the nuclei are spherical, an hypothesis which might not hold for heavier nuclei, such as those studied here.

B. Symmetric and asymmetric modes

One striking feature of the fragment mass distributions present in Fig. 1 is that the asymmetric fission contribution is much more evident for ^{238}U than for the other nuclei studied, despite the fact that they have similar masses. This behavior can be explained by taking into account the empirical expression for the critical value of the fissility parameter defined by Chung *et al.* [31]:

$$(Z^2/A)_{cr} = 35.5 + 0.4(Z_f - 90). \quad (9)$$

where Z_f is the atomic number of the fissioning nucleus. According to Chung *et al.* [31], for nuclei with values of Z^2/A greater than the critical value, the symmetric fission mode is dominant, while for nuclei with smaller values the main fission channel leads to asymmetric fragment distribution. The higher the fissility parameter, with respect to the critical value, the higher is the probability to obtain a symmetric mass distribution.

The critical fissility parameter $(Z^2/A)_{cr}$ for ^{241}Am, ^{238}U, and ^{237}Np are 37.5, 36.3, and 36.7, respectively, while the average fissility parameter, Z^2/A, is 39.7 ($A = 227$, $Z = 95$) for ^{241}Am, 37.3 ($A = 227$, $Z = 92$) for ^{238}U, and 38.7 ($A = 223$, $Z = 93$) for ^{237}Np.

The smallest difference between Z^2/A and $(Z^2/A)_{cr}$ is found for ^{238}U and it could explain the larger contribution of asymmetric fission in the mass distribution for this nucleus. A lower Z^2/A value for ^{238}U is a consequence of the pre- and postequilibrium emissions, which result in compound and fissioning nucleus mass distributions rather different from those obtained for the other target nuclei. We present in Table II the average mass of the compound nucleus A_{CN}, the average fissioning nucleus mass A_f, and the average mass of fission fragments after evaporation, A_{ff}, for the three cases studied here. The comparison between them shows that the number of prescission neutrons is higher for ^{238}U, which could be related to a lower excitation energy of the fissioning nucleus. This is confirmed by the lower number of postscission neutrons for uranium when compared to the other nuclei. Thus, although the total number of neutrons emitted is approximately the same for all nuclei studied here, the prescission evaporation chain is longer for ^{338}U. This causes not only a lower excitation energy, but also the formation of a lighter fissioning system, with a lower Z^2/A parameter, explaining the more pronounced contribution of asymmetric fission for ^{238}U as compared to those for ^{241}Am and ^{237}Np.

C. Proton and neutron emissions

Besides the fragment mass distribution, it is also interesting to analyze some aspects of the fission process related to charge distributions and particle emission of the fragments. The charge distribution for an isobar chain with mass number A,

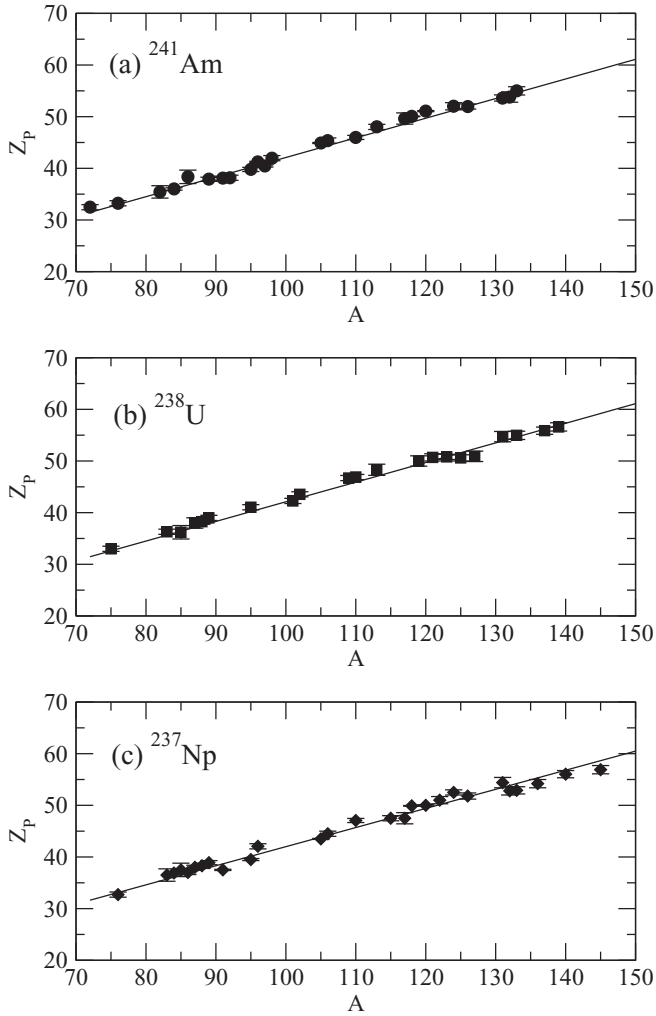

FIG. 3. The most probable charge Z_p for (a) ^{241}Am, (b) ^{238}U, and (c) ^{237}Np targets, respectively. The calculations by CRISP are given by the solid line while the filled symbols are experimental data.

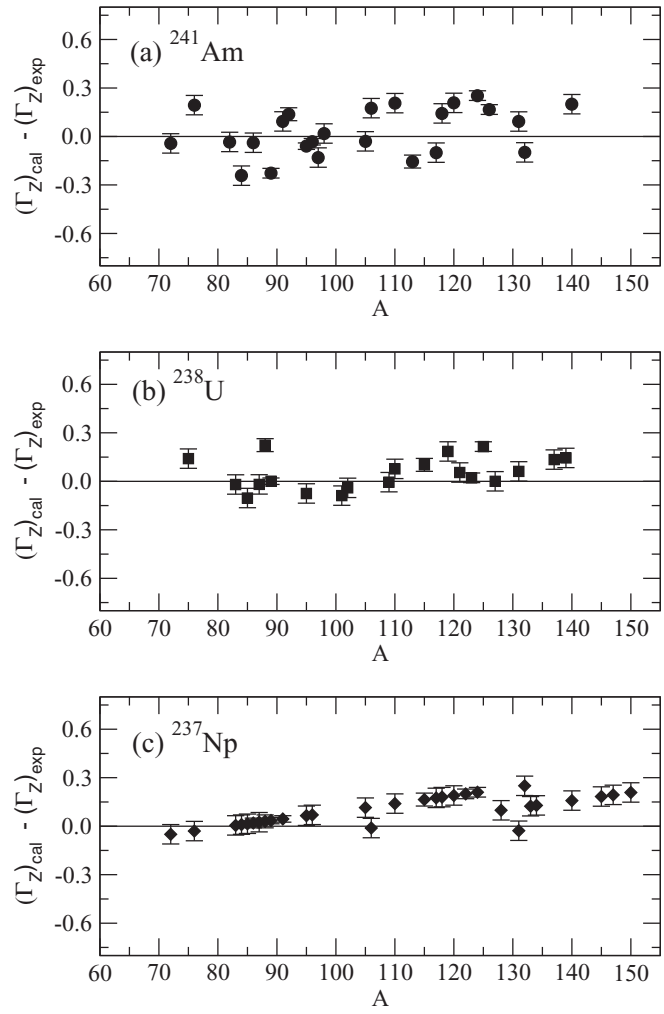

FIG. 4. The deviation between the experimental width of charge distribution and the values calculated by the CRISP code for (a) ^{241}Am, (b) ^{238}U, and (c) ^{237}Np targets.

from a fissioning heavy nuclei, is characterized by a Gaussian shape given by Eq. (3), with parameters, Z_p and Γ_z, where Z_p and Γ_z are the most-probable charge and the corresponding width of the distribution. In Fig. 3 we show the comparison between experimental and calculated values with the CRISP code for Z_p as a function of A. As can be seen, the calculation reproduces quite well the experimental data and both of them show a clear linear dependence of Z_p with A, as expected by Eqs. (4) and (5) [22]. In Fig. 4 we plot the difference between the calculated width Γ_p and experimental values. We observe that for ^{241}Am and ^{238}U, the data fluctuates around zero, as one would expect, with standard deviations of 3.4 and 2.6, respectively. In the case of ^{237}Np, although the values are close to zero, the results show a clear linear dependence of the parameter Γ_p with A. In general, the calculated values are in good agreement with the experiment, especially for the fragments in the low and medium mass regions. In the case of ^{237}Np, the calculations systematically overestimate the width of the isotopic distributions in the range of medium and high masses.

With the CRISP code we can also obtain the average number of pre- and post-scission emitted neutrons, which are reported in Table II. The sum of these two contributions gives the average number of emitted neutrons, which can be compared with the experimental values, also shown in Table II. We observe good agreement between calculated and experimental values, showing that the theoretical predictions for the emission of neutrons are correct.

The analysis of neutron emissions and atomic number distributions shows that the CRISP code gives a good description of the mechanisms for emissions of nucleons in the pre- and postequilibrium stages of the nuclear reaction. It is important to note that the number of emitted nucleons is directly related to the excitation energy of the compound nucleus formed in the reaction, therefore, we can conclude that the excitation energies, as calculated by CRISP, are also supported by the experimental results. The present analysis also indicates that our theoretical model gives a good description of the dynamical process taking place inside the nucleus during reactions at intermediate energies.

IV. CONCLUSION

In this work, an analysis of the fragment mass distributions obtained in the fission of ^{241}Am, ^{238}U, and ^{237}Np induced by 660 MeV protons is presented. The analysis is performed by comparing the results from a Monte Carlo calculation with the CRISP code with experimental data from Ref. [1,2]. We show that the CRISP code can give a reliable description of the fission dynamics for the reactions studied here. In fact, the mass distributions for fission fragments are correctly described by considering three fission modes, one symmetric and two asymmetric, for all three targets studied. The evaporation of fission fragments is also considered, and we found that this mechanism is relevant for the description of the final fragment masses. The pre- and postscission neutron emission and the atomic number distributions were also analyzed, and we show that calculations and experiments are in good agreement. The information of pre- and postscission neutron emissions is important in explaining the different relative contribution of asymmetric fission with respect to symmetric fission for uranium when compared to the other two target nuclei.

ACKNOWLEDGMENTS

G.K. is grateful to Fundação de Amparo à Pesquisa do Estado de São Paulo (FAPESP) 2011/00314-0, and to International Centre for Theoretical Physics (ICTP) under the Associate Grant Scheme. A.D. acknowledge the partial support from CNPq under grant 305639/2010-2 and FAPESP under grant 2010/16641-7. E.A. acknowledge the support from FAPESP under grant 2012/13337-0. We thank Prof. Wayne Seale for reviewing the text.

[1] G. S. Karapetyan, A. R. Balabekyan, N. A. Demekhina, and J. Adam, Phys. At. Nucl. **72**, 911 (2009).
[2] A. R. Balabekyan, G. S. Karapetyan, N. A. Demekhina *et al.*, Phys. At. Nucl. **73**, 1814 (2010).
[3] A. Deppman, S. B. Duarte, G. Silva *et al.*, J. Phys. G: Nucl. Part. Phys. **30**, 1991 (2004).
[4] T. Kodama, S. B. Duarte, K. C. Chung, and R. A. M. S. Nazareth, Phys. Rev. Lett. **49**, 536 (1982).
[5] M. Goncalves, S. dePina, D. A. Lima *et al.*, Phys. Lett. B **406**, 1 (1997).
[6] A. Deppman, O. A. P. Tavares, S. B. Duarte *et al.*, Phys. Rev. Lett. **87**, 182701 (2001).
[7] A. Deppman, O. A. P. Tavares, S. B. Duarte *et al.*, Comp. Phys. Comm. **145**, 385 (2002).
[8] A. Deppman, O. A. P. Tavares, S. B. Duarte, J. D. T. Arruda-Neto, M. Gonçalves, V. P. Likhachev, and E. C. deOliveira, Phys. Rev. C **66**, 067601 (2002).
[9] A. Deppman, G. Silva, S. Anefalos *et al.*, Phys. Rev. C **73**, 064607 (2006).
[10] I. Gonzalez, C. Barbero, A. Deppman *et al.*, J. Phys. G: Part. Nucl. **38**, 115105 (2011).
[11] S. A. Pereira *et al.*, Nucl. Sci. Eng. **159**, 102 (2008).
[12] S. Anefalos, A. Deppman, G. Silva *et al.*, Braz. J. Phys. **35**, 912 (2005).
[13] S. T. Mongelli, J. R. Maiorino, S. Anefalos *et al.*, Braz. J. Phys. **35**, 894 (2005).
[14] V. F. Weisskopf and D. H. Ewing, Phys. Rev. **57**, 472 (1940).
[15] U. Brosa, S. Grossman, and A. Muller, Z. Naturforsch. A **41**, 1341 (1986).
[16] K. Z. Schmidt and B. Jurado, Phys. Procedia **31**, 147 (2012).
[17] E. Andrade-II, J. C. M. Menezes, S. B. Duarte *et al.*, J. Phys. G: Part. Nucl. **38**, 085104 (2011).
[18] E. Andrade-II, J. C. M. Menezes, S. B. Duarte *et al.*, EPJ Web of Conferences **21**, 10001 (2012).
[19] A. Deppman, E. Andrade-II, P. C. R. Rossi *et al.*, Sci. Tech. Nucl. Instal. **2012**, 480343 (2012).
[20] E. Andrade-II, E. Freitas, O. A. P. Tavares *et al.*, *XXXI Workshop on Nuclear Physics in Brazil* (AIP, New York, 2009) [AIP Conf. Proc. **1139**, 64 (2009)].
[21] W. Younes, J. A. Becker, L. A. Bernstein *et al.*, *Nuclear Physics in the 21st Century: International Nuclear Physics Conference (INPC 2001)* (AIP, New York, 2001) [AIP Conf. Proc. **610**, 673 (2001)].
[22] H. Kudo, M. Maruyama, M. Tanikawa, T. Shinozuka, and M. Fujioka, Phys. Rev. C **57**, 178 (1998).
[23] M. C. Duijvestijn, A. J. Koning, J. P. M. Beijers, A. Ferrari, M. Gastal, J. van Klinken, and R. W. Ostendorf, Phys. Rev. C **59**, 776 (1999).
[24] F. J. Hambsch *et al.*, Nucl. Phys. A **709**, 85 (2002).
[25] F. J. Hambsch *et al.*, Nucl. Phys. A **726**, 248 (2003).
[26] T. Ohtsuki, Y. Hamajima, K. Sueki, H. Nakahara, Y. Nagame, N. Shinohara, and H. Ikezoe, Phys. Rev. C **40**, 2144 (1989).
[27] V. M. Maslov, Nucl. Phys. A **717**, 3 (2003).
[28] M. G. Itkis *et al.*, Z. Phys. A **320**, 433 (1985).
[29] I. V. Pokrovsky *et al.*, Phys. Rev. C **62**, 014615 (2000).
[30] A. Deppman, E. Andrade-II, V. Guimarães, G. S. Karapetyan, and N. A. Demekhina, Phys. Rev. C **87**, 054604 (2013).
[31] C. Chung and J. J. Hogan, Phys. Rev. C **25**, 899 (1982).
[32] V. A. Rubchenya, Phys. Rev. C **75**, 054601 (2007).
[33] N. A. Demekhina and G. S. Karapetyan, Phys. At. Nucl. **71**, 27 (2008).
[34] N. A. Demekhina and G. S. Karapetyan, Phys. At. Nucl. **73**, 24 (2010).
[35] T. Fukahori, O. Iwamoto, and S. Chiba, in *Proceedings of the Seventh International Conference on Nuclear Criticality Safety, ICNC2003*, JAERI-conf, 2003-019 (pts. 1-2), edited by Nihon Genshiryoku Kenkyuujo and Nihon Genshiryoku Gakkai (Japan Atomic Energy Research Institute, Tokai-mura, Japan, 2003), p. 144.